Sensors & Transducers, Vol. 154, Issue 7, July 2013, pp. 174-182

www.sensorsportal.com

Sensors & Transducers

http://www.sensorsportal.com

Adaptive Regulation of the Flying Height Based on Hybrid Actuator in Near-field Optical Disk Drives

Yang Li, * Zhizheng Wu, Qingxi Jia, Mei Liu
Department of Precision Mechanical Engineering, Shanghai University, 200072, China
* Tel.: 86-2156331783
* E-mail: zhizhengwu@shu.edu.cn

Received: 28 April 2013 /Accepted: 19 July 2013 /Published: 31 July 2013

Abstract: In the next generation near-field optical data storage systems, higher data transfer rate and higher data density require the optical pickup head to maintain a constant sub-micrometer flying height above the rotating disk surface without any collisions. However, suspension vibration and force disturbance, as well as disk vibration make it difficult to maintain the desired flying height during disk operation in the near-field optical disk drives (ODD). It is proposed in this paper to design a hybrid actuator system which combines both advantages of the flying slide used in hard disk drives and the voice coil actuator used in optical disk drives. Then based on the developed model of the hybrid actuator, an adaptive regulation approach is proposed to regulate the flying height at its desired value, despite the unknown vibrations and the unknown force disturbance. The performance of the proposed approach is analyzed and simulation results are presented to illustrate the capability of the proposed adaptive regulation approach to achieve and maintain the desired flying height. *Copyright © 2013 IFSA.*

Keywords: Optical data storage, Near-field, Flying height, Hybrid actuator, Adaptive regulation.

1. Introduction

Optical data storage has played a crucial role in the information society. With the exploding amount of data being generated for preservation, new storage technology with higher storage density and higher data transfer rate are needed [1]. Near-field recording (NFR) breaking through the light diffraction limit represents a promising technique for optical data recording with a high storage density more than 150 GB/inch^2 in theory. In near field recording, the flying height (optical head-disk spacing) will drop down to less than 100 nm which limits the application of existing far-field recording technology in DVD system. Furthermore, as the flying height drops to deep submicron, the optical pickup head is subject to intermittent contact with the disk surface, which will affect the durability of the pickup head and the disk surface [2-4]. Considering the proven technique of flying head application in hard disk drives (HDD), which can effectively eliminate the collision phenomenon, a hybrid actuator system combining the flying head technology with piezoelectric actuator or voice coil actuator has been suggested for the ultra-high density optical disk drive system [5].

As the optical disk rotates, the flying height varies with time due to a number of factors, including optical disk vibration and force interference, which can significantly affect the reliability of the read and

write operations. One of the major issues associated with the design of a flying height regulation system is the fact that all the sources of flying height variations have unknown and possibly time varying properties. And the traditional approach whereby a controller is designed based on a known model of excitations can't be used in this case. Therefore, it is highly desirable to design an effective control system to suppress these flying height variations [6, 7].

It is proposed in this paper to use an adaptive controller design approach to achieve flying height regulation despite the lack of information on the causes of the flying height variations. The proposed approach comprises two main steps. Firstly, a Q parameterized set of stabilizing controllers is constructed. Then the parameter in the expression of stabilizing controllers is tuned online so that the controller converges to the desired controller needed to achieve regulation [8-10]. In the following, the head-disk interface dynamical model of the hybrid actuator system is first developed, then the adaptive regulator is designed to attenuate the unknown exogenous disturbances. Simulation results are finally presented to illustrate the capability of the proposed adaptive regulation approach to maintain the desired flying height.

2. Dynamical Model for the Head-disk Interface

In the hybrid actuator, the flying slider is similar to those used with HDD except that the objective lens (OL) focuses a laser beam on the bottom of the solid immersion lens (SIL) mounted on the slider to read and write data on the disk. As the disk rotates, it generates an air bearing surface (ABS), which provides a lift force to keep the slider and consequently the pickup head at the desired flying height above the disk surface. Fig. 1 illustrates the schematic view of the proposed actuator structure. The suspension assembled to the end of the optical flying head (OFH) which could be attached on the bobbin of an actuator generally found in DVD.

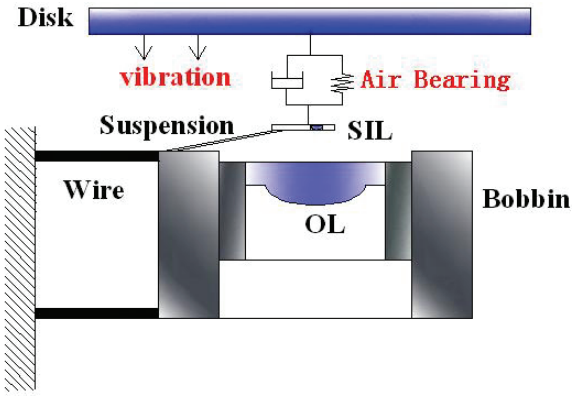

Fig. 1. Schematic view of the hybrid actuator.

Under the action of the ampere force, the moving part attached to the suspension wires takes the OL to move in the flying height direction. In the range of working frequency, the dynamical model for voice coil actuator can be simplified to one-dimensional spring-damping system (Fig. 2 a). Its dynamics and electrical equation is established as follows:

$$\begin{cases} F = m_t\ddot{x} + c_s\dot{x} + k_s x \\ u = e + Ri + L\dot{i} \\ F = Ki \\ e = K\dot{x} \end{cases}, \quad (1)$$

where F is the coil ampere force, m_t is the mass of the actuator, x is the actuator displacement in the flying height direction, c_s is the damping coefficient, k_s is the spring stiffness, u is the coil input voltage, e is the coil induced electromotive force, R is the coil resistance, L is the coil inductance (in the working frequency range, L is normally neglected as $L = 0$), K is the scale factor, and i is the coil instantaneous current.

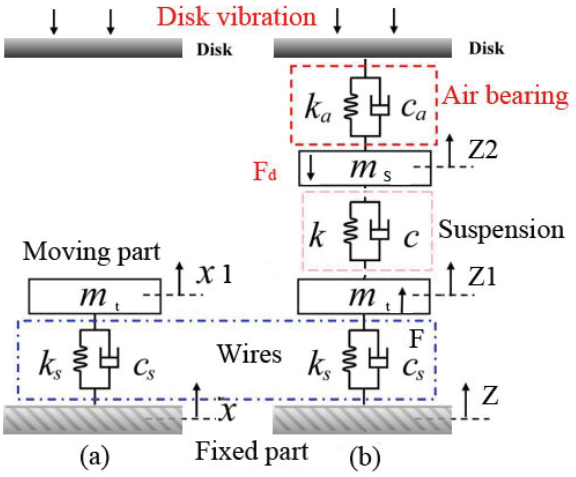

Fig. 2. Lumped model of the hybrid actuator (a) without ABS, (b) with ABS.

In the hybrid actuator, the dynamic coefficients in air bearing play an important role in determining the dynamic characteristics of an air bearing system, like smaller head-disk spacing and less flying height fluctuation. We define that the force F_e represents the sum of external forces applied to the suspension system (including the slider) and can be represented as:

$$F_e = F_a + F_d - F = \iint_A (P - P_a)dxdy + F_d - F . \quad (2)$$

The force F_a which is governed by the pressure distribution $p(x, y)$ and ABS area A corresponds

to the aerodynamic force exerted on the slider during normal operation. The force F represents the actuator force that will be used to regulate the flying height of the slider. F_d represents force disturbances which normally can be expressed as a linear combination of sinusoidal signals.

Although the air bearing of the slider is nonlinear and its stiffness is distributed, the dynamics of the system vibrating around the steady state can be analyzed and verified by simulation or experiment to obtain linearized mode shapes, modal frequencies, and damping ratios [11, 12]. One degree of freedom system, which simplifies the air bearing model as a spring-damper system in the optical disk drives (ODD) system, has been used in [13]. In order to simplify the presentation, in this paper only the degree of freedom in vertical direction, representing the motion in the z direction perpendicular to the disk surface, is considered (Fig. 2.b) and we assume that the slide is vibrating around the steady state. z_1 represents the displacement of the actuator bobbin moving part; z_2 represents the displacement of the slider. The diagram in Fig. 2 shows the slider with mass m_s. The slider is attached to a suspension represented by a spring-damper system where k and c are the corresponding spring stiffness and damping coefficient. The air bearing effects of the front and rear pads are simplified by a lumped linear spring k_a and damper c_a.

The dynamic equation of motion for the head-disk interface (Fig. 2 b) can be written as:

$$\begin{cases} m_s\ddot{z}_2+(c_a+c)\dot{z}_2-c\dot{z}_1+(k_a+k)z_2-kz_1 \\ -c_a\dot{z}_d-k_az_d=-F_d \\ m_t\ddot{z}_1+(c_s+c)\dot{z}_1-c\dot{z}_2+(k_s+k)z_1-kz_2=F \\ u=e+Ri \\ F=Ki \\ e=K\dot{z}_1 \end{cases}. \quad (3)$$

The measurable output y, to be fed to the controller, is defined to be the deviation of the flying height, which is the deviation of distance between the pickup head and the disk surface:

$$y=z_d-z_2,$$

where the wavy external vibration z_d is expressed as a linear combination of sinusoidal functions:

$$z_d=\sum_k c_k\cos(2\pi f_k t+\phi_k), \quad (4)$$

with amplitudes c_k, frequencies f_k, and phases ϕ_k, $k=1,2,\ldots$ The amplitude c_k decreases as the frequency f_k increases [14-16].

The dynamic equation of motion for the head-disk interface can be written as the state-space model:

$$\begin{cases} \dot{z}_1=z_3 \\ \dot{z}_2=z_4 \\ \dot{z}_3=1/m_t\left[-(k+k_s)z_1+kz_2-(c+c_s+K^2/R)z_3\right] \\ \quad +1/m_t\left[-cz_4+Ku/R\right] \\ \dot{z}_4=1/m_s\left[kz_1-(k+k_a)z_2+cz_3-(c+c_a)z_4-F_d\right] \\ \quad +1/m_s\left[c_a\dot{z}_d+k_az_d\right] \\ y=z_2 \end{cases} \quad (5)$$

In the ODD systems, the distance between the pickup head and the disk surface could be inferred from the strength of the read-back signal from a magneto-resistive or optical detecting element [17]-[19]. The deviation of the actual flying height from the desired flying height can be represented as a performance variable e. Therefore, we have that:

$$e=z_d-z_2.$$

Define now the following disturbance vector:

$$w=\begin{bmatrix}(F_d-c_a\dot{z}_d)/m_s \\ z_d\end{bmatrix}.$$

Define $z=[z_1 \quad z_2 \quad z_3 \quad z_4]'$ and the state-space model with disturbance inputs can be written as:

$$\begin{cases} \dot{z}=A_cz+B_cu+E_cw \\ y=C_cz+D_cw \\ e=C_cz+D_cw \end{cases}, \quad (6)$$

where

$$A_c=\begin{bmatrix} 0 & 0 & 1 & 0 \\ 0 & 0 & 0 & 1 \\ -(k+k_s)/m_t & k/m_t & -(c+c_s+K^2/R)/m_t & -c/m_t \\ k/m_s & -(k+k_a)/m_s & c/m_s & -(c+c_a)/m_s \end{bmatrix},$$

$$B_c=\begin{bmatrix}0\\0\\K/(m_tR)\\0\end{bmatrix},\ C_c=[0 \quad -1 \quad 0 \quad 0],$$

$$D_c=[0 \quad 1],\ E_c=\begin{bmatrix}0&0\\0&0\\0&0\\-1&k_a/m_s\end{bmatrix}.$$

Therefore, the flying height regulation problem is transformed into a disturbance cancellation problem for the system given in (6), where the objective is to find a controller that will drive the system performance variable e to zero asymptotically.

3. Design of Adaptive Regulation

3.1. Observe- based Feedback Controller

The construction of a parameterized set of stabilizing controllers for the plant is the key to the controller design. Each controller within this set has the structure of an observer-based controller whose dynamics is augmented with a stable mapping, or parameter Q, which can be chosen as desired [8-10].

Consider the discrete-time linear system model of (6) to be given by:

$$\sum: \begin{cases} x(k+1) = Ax(k) + Bu(k) + E\,w(k), \\ \quad x(0) = x_0 \\ y(k) = C_y x(k) + D_{yw} w(k) \\ e(k) = C_e x(k) + D_{ew} w(k) \end{cases}, \quad (7)$$

where the transformational relation is $A = e^{A_c T}$, $B = \int_0^T e^{A_c \tau} d\tau B_c$, $E = \int_0^T e^{A_c \tau} d\tau E_c$, $C_e = C_y = C_c$, $D_{yw} = D_{ew} = D_c$, T is the sampling period and $x \in \mathbf{R}^n$ is the state vector, $u \in \mathbf{R}$ is the control input (coil input voltage), $y \in \mathbf{R}$ is the measurement signal to be fed to the controller, and $e \in \mathbf{R}$ is the performance variable (deviation of the actual flying height) to be regulated. For the system (6), it is desired to construct an output feedback controller to regulate the performance variable against the unknown external signal $\omega(k)$ such that $\lim_{k\to\infty} e(k) = 0$.

Consider now an observer based controller:

$$\Sigma_c: \begin{cases} \hat{x}(k+1) = A\hat{x}(k) + Bu(k) \\ \qquad\quad + L[\hat{y}(k) - y(k)], \\ u(k) \quad = K\hat{x}(k), \quad \hat{x}(0) = \hat{x}_0 \end{cases}, \quad (8)$$

where $\hat{x}(k)$ is the estimate of the plant state vector and $\hat{y}(k) = C_y \hat{x}(k)$ is an estimate of the plant output y. The matrix K and L are such that $(A + BK)$ and $(A + LC_y)$ are stability matrices, respectively. Hence, we have:

$$\Sigma_c: \begin{cases} \hat{x}(k+1) = (A + LC_y)\hat{x}(k) \\ \qquad\quad + Bu(k) - Ly(k), \\ u(k) \quad = K\hat{x}(k), \quad \hat{x}(0) = \hat{x}_0 \end{cases}. \quad (9)$$

Let $\tilde{x}(k) = \hat{x}(k) - x(k)$ denote the state estimation error. Then, the closed loop system dynamics can be expressed as:

$$\begin{bmatrix} x(k+1) \\ \tilde{x}(k+1) \\ e(k) \end{bmatrix} = \begin{bmatrix} (A+BK) & BK & E \\ 0 & (A+LC_y) & (-E - LD_{yw}) \\ C_e & 0 & D_{ew} \end{bmatrix} \begin{bmatrix} x(k) \\ \tilde{x}(k) \\ w(k) \end{bmatrix}. \quad (10)$$

3.2. Parameterization of a Set of Stabilizing Controllers

The Q parameterization of stabilizing controllers is a method that allows the construction of sets of stabilizing controllers for a given linear time-invariant system, where each controller is expressed as a function of a stable mapping, or parameter. The resulting closed loop system with a parameterized controller is then represented as shown in Fig. 3, where the parameterized controller is now a function of a fixed system J, and a stable parameter Q that can be chosen as desired. Then the J block is given by:

$$\begin{cases} \hat{x}(k+1) = (A + LC_y + BK)\hat{x}(k) \\ \qquad\quad -Ly(k) + By_Q(k) \\ u(k) = K\hat{x}(k) + y_Q(k) \\ y(k) - \hat{y}(k) = y(k) - C_y\hat{x}(k) \end{cases}, \quad (11)$$

whereas parameter Q is given by:

$$\begin{cases} x_Q(k+1) = A_Q x_Q(k) + B_Q\left(y(k) - \hat{y}(k)\right) \\ y_Q(k) = C_Q x_Q(k) \end{cases}. \quad (12)$$

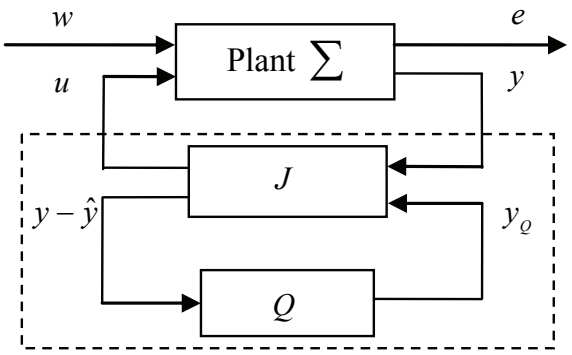

Fig. 3. Closed loop system with a Q - parameterized controller.

The plant Σ and the block J can be combined into an augmented plant T. The dynamics of the augmented plant T can be represented as follows:

$$\begin{bmatrix} x(k+1) \\ \tilde{x}(k+1) \\ e(k) \\ y(k)-\hat{y}(k) \end{bmatrix} = \begin{bmatrix} A+BK & BK & E & B \\ 0 & A+LC_y & -E-LD_{yw} & 0 \\ C_e & 0 & D_{ew} & 0 \\ 0 & -C_y & D_{yw} & 0 \end{bmatrix} \begin{bmatrix} x(k) \\ \tilde{x}(k) \\ w(k) \\ y_Q(k) \end{bmatrix}. \quad (13)$$

Therefore, we have that:

$$\begin{bmatrix} e(k) \\ y(k)-\hat{y}(k) \end{bmatrix} = \begin{bmatrix} T_{11} & T_{12} \\ T_{21} & T_{22} \end{bmatrix} \begin{bmatrix} w(k) \\ y_Q(k) \end{bmatrix}, \quad (14)$$

where

$$T_{11} := \begin{bmatrix} A_{11} & E_{11} \\ C_{11} & D_{11} \end{bmatrix} = \left[\begin{array}{cc:c} A+BK & BK & E \\ 0 & A+LC_y & -E-LD_y \\ \hdashline C_e & 0 & D_e \end{array}\right]$$

$$T_{12} := \begin{bmatrix} A_{12} & E_{12} \\ C_{12} & D_{12} \end{bmatrix} = \left[\begin{array}{cc:c} A+BK & BK & B \\ 0 & A+LC_y & 0 \\ \hdashline C_e & 0 & 0 \end{array}\right] = \begin{bmatrix} A+BK & B \\ C_e & 0 \end{bmatrix},$$

$$T_{21} := \begin{bmatrix} A_{21} & E_{21} \\ C_{21} & D_{21} \end{bmatrix} = \begin{bmatrix} A+LC_y & -E-LD_y \\ -C_y & D_y \end{bmatrix},$$

$$T_{22} = 0.$$

Let $W(z)$ and $E(z)$ denote the Z transform of the disturbance input w and the performance variable e respectively. Let E^j, D_{ew}^j, and D_{yw}^j denote the j^{th} columns of the matrices E, D_{ew}, and D_{yw} respectively. Using equation (14), the closed-loop system transfer function can be expressed as:

$$E(z) = F_{T,Q}(z)W(z) = [T_{11} + T_{12}QT_{21}]W(z) = \sum_{j=1}^{s} [T_{11}^j(z) + T_{12}(z)Q(z)T_{21}^j(z)]W_j(z),$$

where

$$T_{11}^j = \begin{bmatrix} A+BK & BK & E^j \\ 0 & A+LC_y & -E^j-LD_{yw}^j \\ C_e & 0 & D_{ew}^j \end{bmatrix},$$

$$T_{21}^j = \begin{bmatrix} A+LC_y & -E^j-LD_{yw}^j \\ -C_y & D_{yw}^j \end{bmatrix}, j = 1,\cdots,s.$$

In this paper the Q parameter is considered as:

$$Q(z) = \sum_{i=1}^{n_Q} \theta_i z^{1-i} F(z),$$

where $F(z) = \dfrac{b_1 z^{s-1} + \cdots + b_s}{z^s + a_1 z^{s-1} + \cdots + a_s}$ is a weighted function used to adjust the dynamic properties of $Q(z)$. Let $\theta = \left[\theta_1, \ldots, \theta_{n_q}\right]^T$ and $n_Q = s + n_q - 1$. A $Q(z)$ state space realization of can then be given as:

$$A_Q = \begin{bmatrix} 0 & \cdots & 0 & 0 & -a_s & 0 & 0 & 0 \\ 1 & \cdots & 0 & 0 & -a_{s-1} & 0 & 0 & 0 \\ \vdots & \ddots & \vdots & \vdots & \vdots & \vdots & \vdots & \vdots \\ 0 & \cdots & 1 & 0 & -a_2 & 0 & 0 & 0 \\ 0 & \cdots & 0 & 1 & -a_1 & 0 & 0 & 0 \\ 0 & \cdots & 0 & 0 & 1 & 0 & 0 & 0 \\ 0 & \cdots & 0 & 0 & 0 & \ddots & 0 & 0 \\ 0 & \cdots & 0 & 0 & 0 & 0 & 1 & 0 \end{bmatrix}_{n_Q \times n_Q},$$

$$B_Q = \begin{bmatrix} b_s \\ b_{s-1} \\ \vdots \\ b_2 \\ b_1 \\ 0 \\ \vdots \\ 0 \end{bmatrix}_{n_Q \times 1}, \quad C_Q = \begin{bmatrix} 0_{1\times(s-1)} & \theta^T \end{bmatrix},$$

where A_Q is a fixed stability matrix, B_Q is a fixed matrix, and the matrix C_Q changes with the parameter vectors θ which can be tuned online using the adaptation algorithm.

3.3. Adaptation Algorithm

In the case where the disturbance input properties are unknown and possibly time varying, it is desired to introduce adaptation in the controller design process. The aim of the adaptation is to tune the parameter vector θ in order to converge to the desired parameter vector θ_0 needed to achieve regulation. Let q^{-l} denote the l time step delay operator, and

$$Q_k = \bar{Q}_k F(q^{-1}),\ \bar{Q}_k = \sum_{i=1}^{n_Q} \theta_i(k-1) q^{1-i}.$$

The performance variable $e(k)$ is then given by:

$$\begin{aligned} e(k) &= [T_{11}(q^{-1}) + \\ &\quad T_{12}(q^{-1})\bar{Q}_k F(q^{-1}) T_{21}(q^{-1})]w(k) \\ &= T_{11}(q^{-1})w(k) + T_{12}(q^{-1})\bar{Q}_k F(q^{-1}) r(k) \end{aligned}, \quad (15)$$

where

$$r(k) = T_{21}(q^{-1})w(k) = y(k) - \hat{y}(k),$$

$r(k)$ is one of the outputs of block J and thus can be obtained at each step k. Let θ_0 be a parameter vector satisfying the interpolation condition and $\bar{Q}_0$ be the Youla parameter that results from using θ_0. The corresponding performance error resulting from $\bar{Q}_0$ can be then written as:

$$e_0(k) = T_{11}(q^{-1})w(k) + \bar{Q}_0 T_{12}(q^{-1})F(q^{-1})r(k),$$

and $\lim_{k\to\infty} e_0(k) = 0$. Define the signals:

$$\bar{e}(k) = [T_{12}(q^{-1})\bar{Q}_k - \bar{Q}_k T_{12}(q^{-1})]F(q^{-1})r(k),$$

and the error:

$$\begin{aligned}\tilde{e}^0(k) &= e(k) - \bar{e}(k) \\ &= T_{11}(q^{-1})w(k) + \bar{Q}_0 T_{12}(q^{-1})F(q^{-1})r(k) \cdot \\ &\quad + \left(\bar{Q}_k - \bar{Q}_0\right)T_{12}(q^{-1})F(q^{-1})r(k)\end{aligned} \quad (16)$$

Define $v_1(k) = T_{12}(q^{-1})F(q^{-1})r(k)$ and the regression vector

$$\phi(k) = [-v_1(k), \cdots, -v_1(k-n_q+1)]^T. \quad (17)$$

Define the estimated parameter vector $\hat{\theta}(k) = [\hat{\theta}_1(k), \cdots, \hat{\theta}_{n_Q}(k)]^T$ and $\tilde{\theta}(k) = \theta_0 - \hat{\theta}(k)$, then the error $\tilde{e}^0(k+1)$ can be written as:

$$\begin{aligned}\tilde{e}^0(k+1) &= \phi^T(k+1)\left(\theta_0 - \hat{\theta}(k)\right) + e_0(k+1) \\ &= \phi^T(k+1)\tilde{\theta}(k) + e_0(k+1)\end{aligned}. \quad (18)$$

The corresponding posteriori error is:

$$\begin{aligned}\tilde{e}(k+1) &= \phi^T(k+1)\left(\theta_0 - \hat{\theta}(k+1)\right) \\ &\quad + e_0(k+1) \\ &= \phi^T(k+1)\tilde{\theta}(k+1) + e_0(k+1)\end{aligned}. \quad (19)$$

The estimation of the unknown parameter vector $\hat{\theta}(\cdot)$ can then be performed using different algorithms such as a gradient adaptation algorithm or recursive adaptive algorithms. For example, the recursive least squares algorithm with a time varying forgetting factor can be given as follows:

$$\begin{aligned}\hat{\theta}(k+1) &= \hat{\theta}(k) + P(k)\phi(k+1)\tilde{e}(k+1) \\ P(k+1) &= \frac{1}{\lambda(k+1)}\left[\begin{array}{l}P(k) - \\ \dfrac{P(k)\phi(k+1)\phi^T(k+1)P(k)}{1+\phi^T(k+1)P(k)\phi(k+1)}\end{array}\right], \\ \tilde{e}(k+1) &= \frac{\tilde{e}^0(k+1)}{1+\phi(k+1)P(k)\phi^T(k+1)}\end{aligned} \quad (20)$$

with $\hat{\theta}(0) = 0$, $P(0) = P_0 > 0$, and where $\lambda(k)$ is a time varying forgetting factor satisfying $0 < \lambda_{\min} \le \lambda(k) \le \lambda_{\max} < 1$.

If it is assumed that the disturbance parameters are piecewise constant and that changes in the parameters are sufficiently spaced in time to allow parameter convergence. Then the algorithm given by (20) yields $\lim_{k\to\infty} \tilde{\theta}(k) = 0$, and the regulation in the adaptive closed loop system against the unknown disturbance w is achieved.

4. Simulation Results

In this section, the simulation results obtained in Matlab/Simulink is presented to show the performance of the adaptive regulation using the hybrid actuator system in maintaining a desired flying height despite the unknown and time varying external disturbances. The different system parameters shown in Fig. 2 are given as follows: $\xi = 0.002$, $k = 4.9N/m$, $\xi_a = 0.07$, $k_a = 1.0\times10^6 N/m$, $\xi_s = 0.1581$, $k_s = 150N/m$, and where $c = 2\xi\sqrt{m_s k}$, $c_a = 2\xi_a\sqrt{m_s k_a}$, $c_s = 2\xi_s\sqrt{m_t k_s}$, ξ is the normal damping ratio of slider suspension, ξ_a is the air bearing damping ratio, and ξ_s is the wire damping ratio.

In the following, a wavy disk vibration given by a linear combination of two sinusoids of frequencies 20 Hz and 30 Hz and force disturbance given by a sinusoid of frequency 20 Hz are considered. The flying height in the equilibrium state is set as 50 nanometers, which also represents the desired flying height during normal disk operation. Firstly, the response of the open loop system to a disk vibration given by $z_d = c_1\sin(2\pi f_1 t)$ with $f_1 = 20$ Hz and $c_1 = 1000$ nm, and force disturbance given by $F_d = c_2\sin(2\pi f_2 t)$ with $f_2 = 20$ Hz and $c_2 = 0.1$ mN, is investigated. As shown in Fig. 4, the simulation results show the pickup head stays steadily at the desired equilibrium flying height despite the unknown disturbances.

Fig. 5 and Fig. 6 show that the disk wavy vibration is the combination of two sinusoids:

$$\phi(k) = [-v_1(k), \cdots, -v_1(k-n_q+1)]^T,$$

where $f_1 = 20$ Hz, $c_1 = 1000$ nm, $f_2 = 30$ Hz and $c_2 = 200$ nm, and force disturbance given by $F_d = c_3\sin(2\pi f_3 t)$ mN where $f_3 = 20$ Hz and the amplitude $c_3 = 0.1$ mN. As shown in Fig. 5 and Fig. 6, the simulation results show the pickup head stays steadily at the desired equilibrium flying position despite the unknown multiple narrow band disturbances.

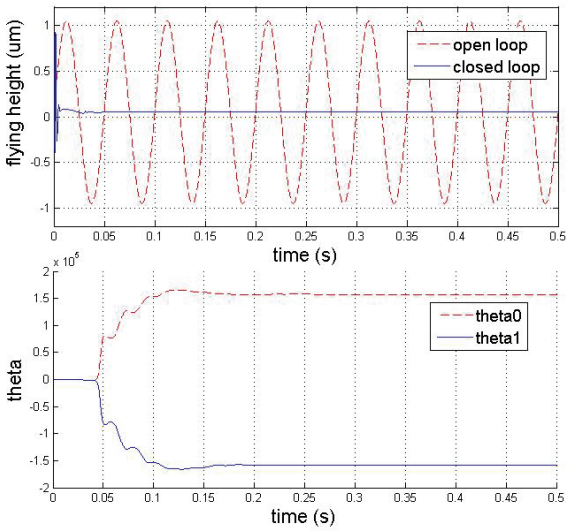

Fig. 4. Adaptive system response with a wavy disk vibration $z_d = 1000\sin(40\pi t)$ nm and force disturbance $F_d = 0.1\sin(40\pi t)$ mN . Top: flying height with open loop (Dashed) and flying height with closed loop (Solid). Bottom: Estimated Q parameters with two thetas.

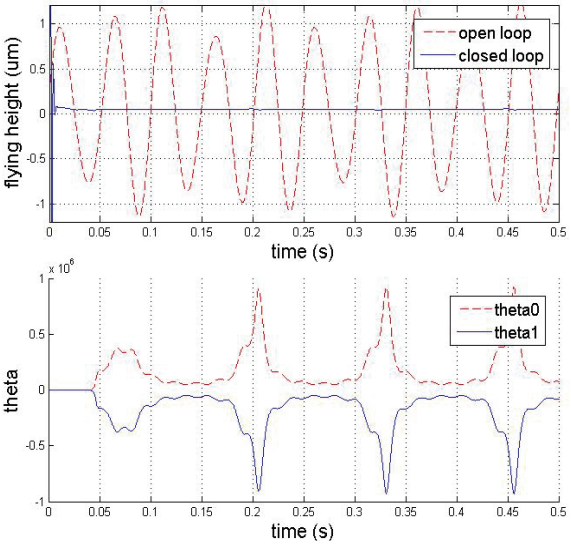

Fig. 5. Adaptive system response with a wavy disk vibration $z_d = 1000\sin(40\pi t) + 200\cos(60\pi t)$ nm and force disturbance $F_d = 0.1\sin(40\pi t)$ mN . Top: flying height with open loop (Dashed) and flying height with closed loop (Solid). Bottom: Estimated Q parameters with two thetas.

The disturbances with a larger number of sinusoids can also be easily accommodated with more parameters in θ. Fig. 7 gives the results for the open loop and the adaptive closed loop systems, respectively, to the disturbance $z_d = 1000\sin(40\pi t) + 200\cos(2\pi f_2 t)$nm with a chirp type evolution of f_2 starting from 20 Hz to 30 Hz. As can be seen in Fig. 7, the chirp disturbance signal is effectively attenuated.

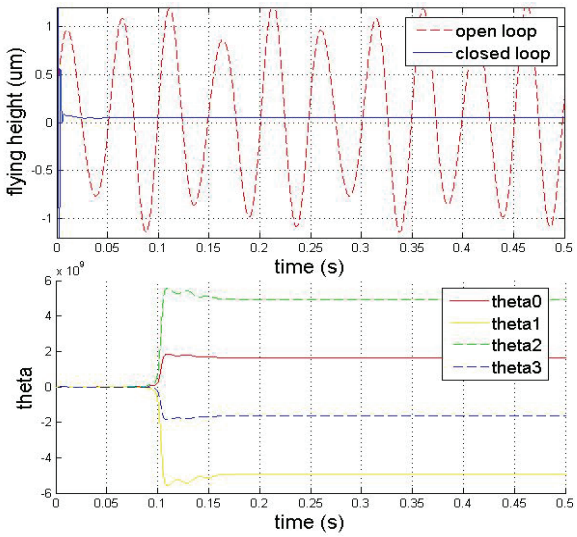

Fig. 6. Adaptive system response with a wavy disk vibration $z_d = 1000\sin(40\pi t) + 200\cos(60\pi t)$ nm and force disturbance $F_d = 0.1\sin(40\pi t)$ mN . Top: flying height with open loop (Dashed) and flying height with closed loop (Solid). Bottom: Estimated Q parameters with four thetas.

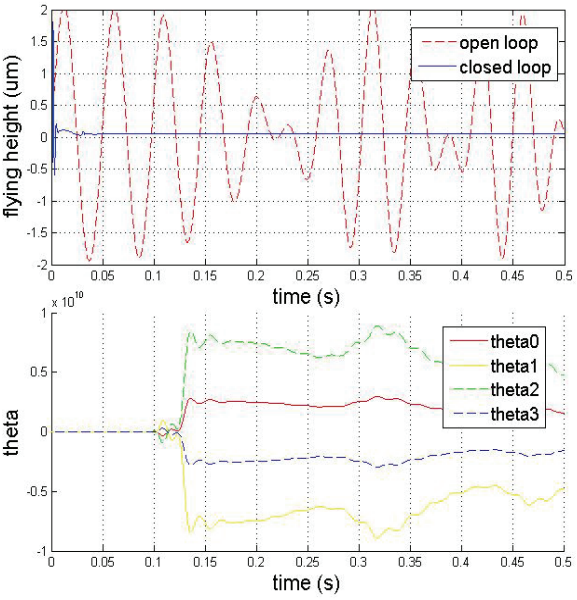

Fig. 7. Adaptive system response to the main wavy disk vibration $z_d = 1000\sin(40\pi t) + 200\cos(2\pi f_2 t)$nm with a chirp type evolution of f_2 starting from 20 Hz to 30 Hz, and force disturbance $F_d = 0.1\sin(40\pi t)$ mN . Top: flying height with open loop (Dashed) and flying height with closed loop (Solid). Bottom: Estimated Q parameters with four thetas.

Fig. 8 shows the case that the main wavy disk vibration is $z_d = 1000\sin(40\pi t) + 200\cos(2\pi f_2 t)$nm with a chirp type evolution of f_2 starting from 20 Hz to 30 Hz, while the force disturbance is divided into

two sections. Before time $t = 0.25$ seconds, the disturbance is represented as a sinusoid $F_d = 0.1\sin(40\pi t)$ mN with the frequency $f = 20$ Hz . At $t = 0.25$ seconds, the disturbance is represented as a sinusoid $F_d = 0.05\sin(60\pi t)$ mN with the frequency $f = 30$ Hz . As shown in Fig. 8, the simulation results show the pickup head stays smoothly at the desired equilibrium flying position even under the case that the disturbance frequency abruptly changes.

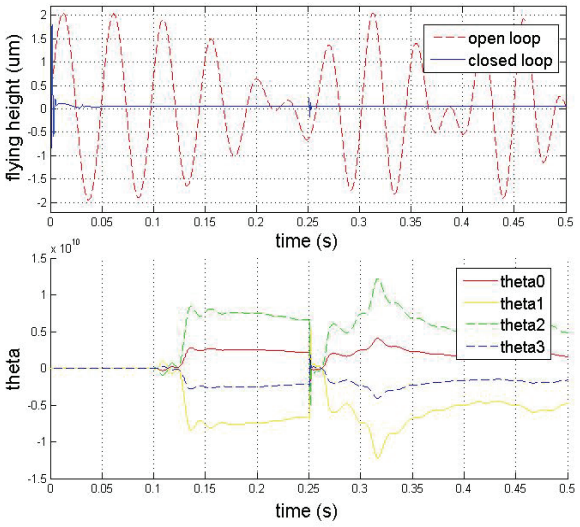

Fig. 8. Adaptive system response to the main wavy disk vibration $z_d = 1000\sin(40\pi t) + 200\cos(2\pi f_2 t)$nm with a chirp type evolution of f_2 starting from 20 Hz to 30 Hz, and step force disturbance $F_d = 0.1\sin(40\pi t)$ mN for $t \le 0.25$ sec, $F_d = 0.05\sin(60\pi t)$ mN for $t \ge 0.5$ sec. Top: flying height with open loop (Dashed) and flying height with closed loop (Solid). Bottom: Estimated Q parameters with four thetas.

5. Conclusions

The reduction in the flying height of the read/write head is critical to increasing the data storage density in optical data storage systems. In this paper, a hybrid actuator system is proposed and an adaptive regulation approach is designed to maintain the desired flying height of the pickup optical head. The dynamical model is first built for the head-disk interface of the hybrid actuator system. Then an adaptive regulator is developed to achieve flying height regulation despite the lack of information on the causes of the flying height variations. The adaptive regulation approach is based on the Q parameterization of stabilizing controllers. The main idea behind the regulation approach is to tune the Q parameter in the expression of stabilizing controllers online in order to converge to the controller that yields regulation. The performance of the proposed approach is illustrated using simulation results showing that the flying height is maintained at the desired value despite the unknown and time varying external disturbances.

Acknowledgements

This work was supported by the National Natural Science Foundation of China (51075254), the Shanghai Pujiang Program (11PJ1404000) and the Innovation Program of Shanghai Municipal Education Commission (11YZ16).

References

[1]. K. Park, Y. Park and N. Park, Prospect of recording technologies for higher storage performance, *IEEE Transactions on Magnetics*, Vol. 47, No. 3, 2011, pp. 539-545.

[2]. K. Ono, and K. Linda, Analysis of bouncing vibrations of a 2-DOF model of tri-pad contact slider over a random wavy disk surface, *ASME Journal of Tribology*, Vol. 123, 2001, pp. 159-167.

[3]. K. Linda, K. Ono, and M. Yamane, Dynamic characteristics and design consideration of a tri-pad slider in the near-contact regime, *ASME Journal of Tribology*, Vol. 124, 2002, pp. 600-606.

[4]. H. Kohira, H. Tanaka, M. Matsumoto, and F. Talke, Investigation of slider vibrations due to contact with a smooth disk surface, *ASME Journal of Tribology*, Vol. 123, 2001, pp. 616-623.

[5]. J. H. Lee, H. Y. Oh, D. G. Gweon, et al. Optical flying head mounted on four wire type actuator, *Sensors and Actuators A*, Vol. 113, 2004, pp. 100-105.

[6]. J. G. Kim, W. C. Kim, H. W. Hwang, et al. Anti-Shock Air Gap Control for SIL Based Near-Field Recording System, *IEEE Transactions on Magnetics*, Vol. 45, 2009, pp. 2244-2247.

[7]. X. Liu, W. Clegg, D. F. L. Jenkins and P. Davey, Head-disk spacing variation suppression via active flying height control, *IEEE Transactions on Instrumentation and Measurement*, Vol. 51, No. 5, 2002, pp. 897-901.

[8]. Z. Wu and F. Ben Amara, Adaptive regulation in bimodal systems: an experimental evaluation, *IEEE Transaction on Control System Technology*, Vol. 18, No. 4, 2010, pp. 885-895.

[9]. Z. Wu, and Ben Amara, F., Adaptive Regulation in Bimodal Linear Systems, *International Journal of Robust and Nonlinear Control,* Vol. 20, 2010, pp. 59-83.

[10]. F. Ben Amara, P. T. Kabamba, and A. G. Ulsoy, Adaptive sinusoidal disturbance rejection in linear discrete-time systems- Part I: Theory, *ASME Journal of Dynamic Systems, Measurement, and Control*, Vol. 121, No. 4, 1999, pp. 648-654.

[11]. Q. H. Zeng and D. B. Bogy, Stiffness and damping evaluation of air bearing sliders and new designs with high damping, *ASME Journal of Tribology*, Vol. 121, 1999, pp. 341-347.

[12]. G. Sheng, B. Liu, and W. Hua, A nonlinear dynamics theory for modeling slider air bearing in hard disk

drives, *Journal of Applied Physics*, Vol. 87, 2000, pp. 6173-6175.
[13]. Y. H. Lee, Y. E. Lee, K. H. Kim, et al., Effect of air bearing surface on shock resistance of optical head for solid immersion lens based near field recording system, *IEEE Transactions on Magnetics*, Vol. 45, No. 5, 2009, pp. 2236-2239.
[14]. B. J. Shi et al., Operational shock simulation of the head-disk assembly of a small-form factor drive, *IEEE Transactions on Magnetics,* Vol. 43, No. 11, 2007, pp. 4042-4047.
[15]. Z. Wu and F. Ben Amara, Flying height control for a 2-DOF tri-pad slider in hard disk drives with switched regulators, *ASME International Mechanical Engineering Congress and Exposition,* Orlando, FL, 2005, pp. 1-10.
[16]. S. H. Lee, D. G. Gweon, Design and control of high precision 3D pickup actuators for near field recording system, *IEEE Transactions on Consumer Electronics*, Vol. 54, No. 4, 2008, pp. 1977-1980.
[17]. X. Feng, F. He, et al., Flying height control of solid immersion lens by slipstream, *Acta Photonica Sinica*, Vol. 34, No. 6, 2005, pp. 927-930.
[18]. Li, X. Liu, W. Clegg, D. F. L Jenkins, and T. Donnelly, Real-time method to measure head disk spacing variation under vibration conditions, *IEEE Transactions on Instrumentation and Measurement*, Vol. 52, No. 3, 2003, pp. 916-920.
[19]. J. Y. Fang, C. H. Tien, H. P. Shieh, P. Herget, J. A. Bain and T. E. Schlesinger, Optical feed-back height control system using laser diode sensor for near field data storage applications, *Journal of Light Wave Technology*, Vol. 25, No. 12, 2007, pp. 3704-3709.